Transient Magnetic Shielding of a Planar Conductive Thin Screen via Exact Image Theory

Giampiero Lovat, Paolo Burghignoli, *Senior Member, IEEE*, Rodolfo Araneo, *Senior Member, IEEE*, and Salvatore Celozzi, *Senior Member, IEEE*

***Abstract*—The exact image theory is here applied to study the transient shielding effectiveness of a canonical shielding configuration, i.e., a small current loop in the presence of a parallel planar thin conductive sheet. In particular, the Green function providing the electromagnetic field produced by a pulsed vertical magnetic dipole in the whole space is derived in a closed analytical form. The recently introduced definitions of transient shielding effectiveness are used to evaluate the shielding properties of the configuration. The derived results allow for calculations in a closed form for simple transient waveforms of the exciting currents.**

***Index Terms*—Time-domain (TD) electromagnetics, transient fields.**

I. Introduction

THE study of low-frequency (time-harmonic) shielding of a loop that is axially perpendicular to a metallic planar shield of infinite extent is a canonical problem in electromagnetic shielding. In fact, two current loops separated by a parallel planar thin conductive sheet is the configuration prescribed in NSA tests [1], [2] and occurs in several EMC practical cases, such as current paths in printed circuit boards.

This canonical configuration has been extensively studied in the past. The first seminal paper by Levy appeared in the 1930 s [3], assumed thin screens, and was based on an extension of the classical eddy-current analysis of Maxwell. In the 1960 s, Moser derived exact integral expressions for the relevant shielding effectiveness (SE), which however required the numerical evaluation of Sommerfeld-type integrals [4]. Quasi-near-field approximations of such expressions were then derived by Bannister for thick [5] and thin [6] screens. Moser's formulation was compared with experimental data and with Schelkunoff's transmission-line approach in [7], and was further extended to evaluate loop-to-loop coupling in [8].

Exact expressions for the on-axis magnetic SE against small electric-current loop sources were derived in [9] for conductive and in [10] for magneto-conductive thins screens. Such expressions were then generalized to screens with arbitrary thickness and constitutive parameters in [11]. A unified wave impedance formula to be used in the transmission-line approach was derived in [12].

However, all these investigations have considered time-harmonic sources, while only recently the problem of the evaluation of the SE for transient waveforms has started to be addressed [13], [14], [15], [16]. In general, the shielding problem in the time domain (TD) can be solved passing through its frequency-domain counterpart and inverse-Fourier transforming the quantities of interest. However, such a procedure is numerically intensive and cumbersome and does not offer any physical insight into the involved transient wave phenomena. In this connection, the authors of [14], [15], and [16], as in [17], [18], and [19], adopted a modified Cagniard-de Hoop (CDH) approach to solve the electromagnetic problem directly in the TD and to obtain analytical or semi-analytical solutions. In fact, while a number of effective numerical approaches have been developed in the TD based on, e.g., the finite-difference TD method or on TD integral equations, analytical methods maintain their importance both for the derivation of benchmark solutions in canonical geometries and for the physical insight that they afford on the involved transient wave phenomena. In addition to the abovementioned classical CDH method [20], [21], [22], it is worth mentioning the double-deformation method developed by Tsang and Kong [23], [24], the Haddon leaky-wave method [25], [26], the modal asymptotic approaches of Felsen and Niu [27], [28], [29], and the TD version of the exact image theory (EIT) of Lindell and Alanen [30], [31], [32] (initially developed for the solution of the Sommerfeld problem [33], [34]) developed by Nikoskinen and Lindell [35].

In this work, we present a TD version of the EIT to analytically solve the abovementioned classical shielding problem directly in the TD (as Nikoskinen did in the 1990s for a simple half-space configuration [35]) showing that an inverse-Fourier transform of the frequency-domain quantities can be made symbolically starting from the EIT expressions. It is here shown that the TD EIT analytically solves the problem in a considerably simpler way compared with the CDH approach. In particular, easy-to-compute expressions for the transient field components of this canonical configuration are derived. In fact, the final integrals expressing such components may be computed analytically giving a closed-form solution (an example is provided considering the z-component of the magnetic field). Other configurations can

Manuscript received 15 May 2023; revised 16 September 2023 and 16 October 2023; accepted 16 October 2023. Date of publication 3 November 2023; date of current version 13 December 2023. *(Corresponding author: Giampiero Lovat.)*

Giampiero Lovat, Rodolfo Araneo, and Salvatore Celozzi are with the Electrical Engineering Division of DIAEE, University of Rome "Sapienza,", 00184 Rome, Italy (e-mail: giampiero.lovat@uniroma1.it; rodolfo.araneo@uniroma1.it; salvatore.celozzi@uniroma1.it).

Paolo Burghignoli is with the Department of Information Engineering, Electronics and Telecommunications, University of Rome "Sapienza," 00184 Rome, Italy (e-mail: paolo.burghignoli@uniroma1.it).

Color versions of one or more figures in this article are available at https://doi.org/10.1109/TEMC.2023.3326190.

Digital Object Identifier 10.1109/TEMC.2023.3326190

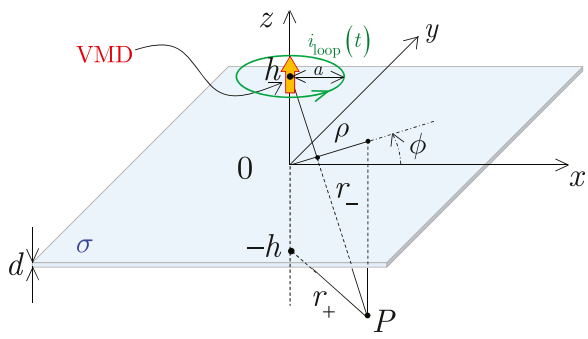

Fig. 1. Electromagnetic configuration considered here: a small transient electric current loop in vacuum, represented as a transient VMD, over an infinite planar screen of thickness d and conductivity σ. The adopted rectangular and cylindrical reference systems are also indicated, along with the two auxiliary distances r_+ and r_- employed in the expressions of the transient potential and fields.

be studied through the proposed formulation (such as the same shielding problem in a coplanar loop set up [36], [37]) and the TD-EIT could in principle be used to characterize other transient problems of EMC interest, such as the transient behavior of grounding systems [38].

The rest of this article is organized as follows. The proposed TD EIT formulation together with its basic assumptions is presented and described in Section II. In Section III, closed-form results for the transient fields are derived. In Section IV, figures of merit for assessing the transient magnetic shielding are introduced and evaluated on the basis of the developed formulation for a specific source waveform. Numerical results are presented in Section V showing the advantages and the limits of the proposed formulations. Finally, Section VI concludes this article.

II. TD EIT Formulation

A. Problem Description and Assumptions

The configuration under analysis is sketched in Fig. 1. It consists of an infinite planar metallic plate with thickness d and conductivity σ. The plate is orthogonal to the vertical z-axis and is excited by a circular loop of radius a carrying a current $i_{\text{loop}}(t)$ with its axis coincident with the z-axis and placed at a distance h from it.

As is well known, when the loop radius a is much smaller than h and the free-space wavelength $\lambda_{0\min}$ at the highest frequency $f_{\max}$ contained in the spectrum of the loop current, the transient loop source is equivalent to a transient z-directed (vertical) magnetic dipole of moment $p_{\text{m}}(t)$ with $p'_{\text{m}}(t) = v(t)\ell$ and

$$v(t)\ell = \mu_0 \pi a^2 \frac{\text{d}i_{\text{loop}}}{\text{d}t} \tag{1}$$

where μ_0 is the magnetic permeability of free space. We, thus, consider a vertical magnetic dipole (VMD) of length ℓ, directed along the z-axis, located at $z = h > 0$ in air carrying a voltage $v(t)$. The source is thus expressed as

$$\mathbf{j}_{\text{mi}}(\mathbf{r}, t) = v(t)\ell\delta(x)\delta(y)\delta(z-h)\,\mathbf{u}_z\,. \tag{2}$$

Moreover, if the screen is sufficiently thin, it can be modeled as a zero-thickness sheet with surface (transition) admittance $G_{\text{s}} = \sigma d$. In particular, as established in [15], the surface admittance representation is accurate provided that

$$d \ll \frac{1}{\sqrt{2\pi f_{\max}\mu_0\sigma}} \tag{3}$$

where $f_{\max}$ is the high-frequency limit of the spectrum of the dipole waveform.

B. TD Potential Green's Function

As is well known, a VMD excites a purely TE^z field, which in turn can be derived from a z-directed electric vector potential (in the Lorenz gauge) $\mathbf{f}(\mathbf{r}, t) = f_z(\mathbf{r}, t)\mathbf{u}_z$. In particular, in vacuum

$$\begin{aligned}\mathbf{e}(\mathbf{r}, t) &= -\frac{1}{\varepsilon_0}\nabla\times\mathbf{f} = -\frac{1}{\varepsilon_0}\nabla f_z \times \mathbf{u}_z \\ \mathbf{h}(\mathbf{r}, t) &= -\mathbf{u}_z\frac{\partial f_z}{\partial t} + c_0^2\nabla\frac{\partial}{\partial z}\int_0^t f_z(\mathbf{r}, t')\,\text{d}t'\end{aligned} \tag{4}$$

where ε_0 is the permittivity of free space and $c_0 = 1/\sqrt{\mu_0\varepsilon_0}$. Thanks to the rotational symmetry of the configuration around the z-axis, the potential is azimuthally symmetric, i.e., $f_z = f_z(\rho, z, t)\mathbf{u}_z$, where $\rho = \sqrt{x^2+y^2}$. The TD potential f_z is solution of the D'Alembert equation, e.g., in vacuum

$$\nabla^2 f_z - \frac{1}{c_0^2}\frac{\partial f_z}{\partial t} = -\varepsilon_0 v(t)\ell\frac{\delta(\rho)}{2\pi}\,\delta(z-h) \tag{5}$$

subject to appropriate boundary conditions. In the following we aim at deriving analytical expressions for $f_z(\rho, z, t)$. In general, such a potential can be expressed as a time convolution between the source waveform $\varepsilon_0 v(t)\ell$ and the relevant TD scalar Green function $g^F(\mathbf{r}, t)$, i.e., the potential produced by an impulsive impressed magnetic current $\mathbf{j}_{\text{m i}}(\mathbf{r}, t)$. In particular, to derive the TD potential Green function $g^F(\mathbf{r}, t)$ of the problem we assume an impulsive $i_{\text{loop}}(t)$, i.e.,

$$v(t)\ell = I_{\text{m}}\ell\delta(t) \tag{6}$$

with $I_{\text{m}}\ell = 1$ V$\cdot$ m.

1) Reflection Half-Space: As is well known, the spectral-domain Green function $\tilde{G}^F$ for the (spectral) electric potential $\tilde{F}_z$ produced by the source in (2)–(6) can be written, for $z > 0$, as [39]

$$\begin{aligned}\tilde{G}^F(\omega; k_\rho; z) &= \frac{1}{2\text{j}k_z}\left[\text{e}^{-\text{j}k_z|z-h|} + R_{\text{TE}}\,\text{e}^{-\text{j}k_z(z+h)}\right] \\ &= \tilde{G}^F_{\text{inc}}(\omega; k_\rho; z) + \tilde{G}^F_{\text{r}}(\omega; k_\rho; z)\end{aligned} \tag{7}$$

where

$$k_z = k_z(\omega; k_\rho) = \sqrt{k_0^2 - k_\rho^2} \tag{8}$$

with $k_0 = \omega/c_0$ and

$$R_{\text{TE}} = R_{\text{TE}}(\omega; k_\rho) = -\frac{1}{1+\frac{2k_z}{k_0\hat{G}_{\text{s}}}} \tag{9}$$

with $\hat{G}_{\text{s}} = \eta_0 G_{\text{s}}$, where $\eta_0 = \sqrt{\mu_0/\varepsilon_0}$.

The free-space term $\tilde{G}^F_{\text{inc}}$ in (7) gives rise to the well-known incident scalar Green function for a point source in free space, i.e.,

$$G^F_{\text{inc}}(\omega;\mathbf{r}) = G^F_0(\omega;r_-) = \frac{\mathrm{e}^{-\mathrm{j}k_0 r_-}}{4\pi r_-} \tag{10}$$

where

$$r_- = \sqrt{\rho^2 + (z-h)^2} \tag{11}$$

which has the following TD counterpart:

$$g^F_{\text{inc}}(\mathbf{r},t) = c_0 \frac{\delta(r_- - c_0 t)}{4\pi r_-}\,. \tag{12}$$

The EIT is based on representing the coefficient R_{TE} as a Laplace transform, so that also the reflected part of $\tilde{G}^F$ can be expressed in terms of point sources (more precisely, as an integral superposition of point sources placed at complex locations). In the present case, from (9), we may write

$$R_{\text{TE}}(\omega;k_\rho) = -\int_0^{+\infty} \mathrm{e}^{-q}\ \mathrm{e}^{-\frac{2k_z}{k_0\hat{G}_{\text{s}}}q}\,\mathrm{d}q \tag{13}$$

so that we obtain

$$\tilde{G}^F_{\text{r}}(\omega;k_\rho;z) = -\int_0^{+\infty} \mathrm{e}^{-q}\,\frac{1}{2\mathrm{j}k_z}\,\mathrm{e}^{-\mathrm{j}k_z\left(z+h-\mathrm{j}\frac{2q}{k_0\hat{G}_{\text{s}}}\right)}\,\mathrm{d}q \tag{14}$$

and, hence,

$$G^F_{\text{r}}(\omega;\mathbf{r}) = -\int_0^{+\infty} \mathrm{e}^{-q}\,G^F_0\left[\omega;D(q;\omega;\mathbf{r})\right]\,\mathrm{d}q \tag{15}$$

where

$$D(q;\omega;\mathbf{r}) = \sqrt{\rho^2 + \left[z+h-\mathrm{j}\zeta_{\text{TE}}(q;\omega)\right]^2} \tag{16}$$

with

$$\zeta_{\text{TE}}(q;\omega) = \frac{2c_0 q}{\omega\hat{G}_{\text{s}}}\,. \tag{17}$$

We, thus, have the sought EIT representation of the reflected Green function of the electric potential in terms of an exponentially converging integral. The integral is a superposition of images located at $-h+\mathrm{j}\zeta_{\text{TE}}$.

The space–time counterpart of $\tilde{G}^F_{\text{r}}$ can be obtained directly through an inverse-Fourier transform of (15), i.e.,

$$g^F_{\text{r}}(\mathbf{r},t) = -\frac{1}{2\pi}\int_{-\infty}^{+\infty}\int_0^{+\infty} \mathrm{e}^{-q}\,G^F_0\left[D(q;\omega;\mathbf{r})\right]\mathrm{d}q\ \mathrm{e}^{\mathrm{j}\omega t}\,\mathrm{d}\omega\,. \tag{18}$$

By interchanging the integrals, we obtain

$$g^F_{\text{r}}(\mathbf{r},t) = -\int_0^{+\infty} \mathrm{e}^{-q}\,G_{\text{c}}(q,t)\,\mathrm{d}q \tag{19}$$

where

$$G_{\text{c}}(q,t) = \frac{1}{2\pi}\int_{-\infty}^{+\infty} G^F_0\left[D(q;\omega;\mathbf{r})\right]\,\mathrm{e}^{\mathrm{j}\omega t}\,\mathrm{d}\omega$$

$$= \frac{1}{2\pi}\int_{-\infty}^{+\infty} \frac{\mathrm{e}^{-\mathrm{j}\frac{\omega}{c_0}\sqrt{\rho^2+\left(z+h-\mathrm{j}\frac{2qc_0}{\omega\hat{G}_{\text{s}}}\right)^2}}}{4\pi\sqrt{\rho^2+\left(z+h-\mathrm{j}\frac{2qc_0}{\omega\hat{G}_{\text{s}}}\right)^2}}\,\mathrm{e}^{\mathrm{j}\omega t}\,\mathrm{d}\omega \tag{20}$$

which can be evaluated in a closed form (details are reported in the Appendix) obtaining

$$G_{\text{c}}(q,t) = \frac{\mathrm{e}^{-\alpha_+ c_0 t q}}{4\pi r_+}\,c_0\left\{\delta(r_+ - c_0 t)\right.$$
$$\left. -\left[\alpha_+ q\mathrm{J}_0(\beta_+ q) + \frac{c_0 t\beta_+ q}{(c_0 t)^2 - r_+^2}\,\mathrm{J}_1(\beta_+ q)\right]H(c_0 t - r_+)\right\} \tag{21}$$

where

$$r_+ = \sqrt{\rho^2 + (z+h)^2} \tag{22}$$

$$\alpha_+ = \frac{2(z+h)}{\hat{G}_{\text{s}} r_+^2} \tag{23}$$

$$\beta_+ = \frac{2\rho\sqrt{(c_0 t)^2 - r_+^2}}{\hat{G}_{\text{s}} r_+^2} \tag{24}$$

and where $\mathrm{J}_n(\cdot)$ is the Bessel function of first kind and of order n and $H(\cdot)$ indicates the unit-step Heaviside function.

The expression in (19) can, thus, also be rewritten as

$$g^F_{\text{r}}(\mathbf{r},t) = -\frac{c_0}{4\pi r_+}\,\delta(r_+ - c_0 t)\int_0^{+\infty} \mathrm{e}^{-\gamma_+ q}\,\mathrm{d}q$$
$$+\frac{c_0}{4\pi r_+}\,\alpha_+ H(c_0 t - r_+)\int_0^{+\infty} \mathrm{e}^{-\gamma_+ q}\,q\mathrm{J}_0(\beta_+ q)\,\mathrm{d}q$$
$$+\frac{c_0^2}{4\pi r_+}\,\frac{\beta_+ t}{(c_0 t)^2 - r_+^2}\,H(c_0 t - r_+)\int_0^{+\infty} \mathrm{e}^{-\gamma_+ q}\,q\mathrm{J}_1(\beta_+ q)\,\mathrm{d}q \tag{25}$$

where

$$\gamma_+ = \alpha_+ c_0 t + 1\,. \tag{26}$$

The integrals in (25) can also be evaluated in simple closed forms using the integral identity [40, 6.621.4], thus obtaining

$$g^F_{\text{r}}(\mathbf{r},t) = -\frac{c_0}{4\pi r_+\gamma_+}\,\delta(r_+ - c_0 t) + \frac{c_0}{4\pi r_+}\,\frac{1}{\left(\gamma_+^2 + \beta_+^2\right)^{3/2}}$$
$$\cdot\left[\alpha_+\gamma_+ + \frac{\beta_+^2 c_0 t}{(c_0 t)^2 - r_+^2}\right]H(c_0 t - r_+)\,. \tag{27}$$

The result further simplifies for source and observation points along the same axis. In fact, for $\rho = 0$, we have

$$g^F_{\text{r}}(0,z,t) = -c_0\hat{G}_{\text{s}}\,\frac{\delta(z+h-c_0 t)}{4\pi\left[2c_0 t + \hat{G}_{\text{s}}(z+h)\right]}$$
$$+ c_0\hat{G}_{\text{s}}\,\frac{H(c_0 t - z - h)}{2\pi\left[2c_0 t + \hat{G}_{\text{s}}(z+h)\right]^2}\,. \tag{28}$$

2) Transmission Half-Space: When $z<0$, the spectral Green function for the electric potential is

$$\tilde{G}^F(\omega;k_\rho;z)=\tilde{G}^F_{\rm t}(\omega;k_\rho;z)=\frac{1}{2{\rm j}k_z}\,{\rm e}^{{\rm j}k_z(z-h)}\,T_{\rm TE} \tag{29}$$

where the TE transmission coefficient is

$$T_{\rm TE}=T_{\rm TE}(\omega;k_\rho)=1+R_{\rm TE}=1-\frac{1}{1+\frac{2k_z}{k_0\hat{G}_{\rm s}}}\,. \tag{30}$$

The TD transmitted Green function for the potential could be obtained immediately from the EIT representation of the reflected potential given above. In fact, the first addend in (30) gives rise to the incident Green function $g^F_{\rm inc}(\mathbf{r},t)$, whereas the second addend gives rise to a term analogous to $g^F_{\rm r}(\mathbf{r},t)$, the only difference being that in all the expressions the term $(z+h)$ should be replaced by $(h-z)$. Therefore,

$$\begin{aligned}g^F_{\rm t}(\mathbf{r},t)=&\frac{c_0}{4\pi r_-}\left(1-\frac{1}{\gamma_-}\right)\delta(r_--c_0t)\\&+\frac{c_0}{4\pi r_-}\frac{1}{(\gamma_-^2+\beta_-^2)^{3/2}}\\&\times\left[\alpha_-\gamma_-+\frac{\beta_-^2c_0t}{(c_0t)^2-r_-^2}\right]H(c_0t-r_-)\end{aligned} \tag{31}$$

where r_- has been defined in (11) while

$$\alpha_-=\frac{2(h-z)}{\hat{G}_{\rm s}r_-^2} \tag{32}$$

$$\beta_-=\frac{2\rho\sqrt{(c_0t)^2-r_-^2}}{\hat{G}_{\rm s}r_-^2} \tag{33}$$

and

$$\gamma_-=\alpha_-c_0t+1\,. \tag{34}$$

It can easily be shown that the result in (31) perfectly coincides with that obtained in [15].

The result further simplifies for source and observation points along the same axis. In fact, for $\rho=0$, we have

$$\alpha_-=\frac{2}{\hat{G}_{\rm s}(h_1-z)} \tag{35}$$

$$\beta_-=0 \tag{36}$$

and therefore,

$$\begin{aligned}g^F_{\rm t}(0,z,t)=&\frac{c_0^2t\delta(h-z-c_0t)}{2\pi\left[2c_0t+\hat{G}_{\rm s}(h-z)\right](h-z)}\\&+\frac{c_0\hat{G}_{\rm s}}{2\pi\left[2c_0t+\hat{G}_{\rm s}(h-z)\right]^2}H(c_0t+h-z)\,.\end{aligned} \tag{37}$$

C. Limiting Cases

It should be noted that in the limit $G_{\rm s}\to 0$ (i.e., free space), it results

$$g^F(\mathbf{r},t)=\frac{c_0}{4\pi r_-}\,\delta(r_--c_0t) \tag{38}$$

whereas for $G_{\rm s}\to+\infty$ (i.e., PEC sheet)

$$g^F(\mathbf{r},t)=\begin{cases}\frac{c_0}{4\pi}\left[\frac{\delta(r_--c_0t)}{r_-}-\frac{\delta(r_+-c_0t)}{r_+}\right], & z>0\\0, & z<0.\end{cases} \tag{39}$$

III. Field Calculation

The TD magnetic potential f_z can be obtained by means of a time convolution between $g^F(\mathbf{r},t)$ and the voltage waveform $\varepsilon_0 v(t)\ell$, i.e.,

$$f_z(\rho,z,t)=\varepsilon_0\int_{-\infty}^{+\infty}g^F(\mathbf{r},t-\tau)\,v(\tau)\,\ell\,{\rm d}\tau\,. \tag{40}$$

Taking into account that $\partial/\partial\phi=0$, from (4), we have

$$\mathbf{e}(\mathbf{r},t)=\mathbf{u}_\phi\frac{\partial}{\partial\rho}\int_{-\infty}^{+\infty}g^F(\mathbf{r},t-\tau)\,v(\tau)\,\ell\,{\rm d}\tau \tag{41}$$

and

$$\begin{aligned}\mathbf{h}(\mathbf{r},t)=&-\varepsilon_0\frac{\partial}{\partial t}\int_{-\infty}^{+\infty}g^F(\mathbf{r},t-\tau)\,v(\tau)\,\ell\,{\rm d}\tau\mathbf{u}_z\\&+\frac{1}{\mu_0}\nabla\frac{\partial}{\partial z}\int_0^t\int_{-\infty}^{+\infty}g^F(\mathbf{r},t'-\tau)\,v(\tau)\ell\,{\rm d}\tau\,{\rm d}t'\,.\end{aligned} \tag{42}$$

In particular, it also results

$$\begin{aligned}h_z(\rho,z,t)=&-\varepsilon_0\frac{\partial}{\partial t}\int_{-\infty}^{+\infty}g^F(\rho,z;t-\tau)\,v(\tau)\,\ell{\rm d}\tau\\&+\frac{1}{\mu_0}\frac{\partial^2}{\partial z^2}\int_0^t\int_{-\infty}^{t'}g^F(\rho,z;t'-\tau)\,v(\tau)\,\ell\,{\rm d}\tau{\rm d}t'.\end{aligned} \tag{43}$$

As an example, let us consider the z-component of the magnetic field along the z-axis ($\rho=0$). First of all, from (28), it is easy to show that

$$\begin{aligned}\int_{-\infty}^{+\infty}g^F_{\rm r}(0,z;t-\tau)\,v(\tau)\,\ell\,{\rm d}\tau=&-\frac{\hat{G}_{\rm s}v(t-T_{\rm r})}{4\pi\left(2+\hat{G}_{\rm s}\right)Z_{\rm r}}\\&+\frac{c_0\hat{G}_{\rm s}}{2\pi}\int_0^{t-T_{\rm r}}\frac{v(\tau)}{\left[2c_0(t-\tau)+\hat{G}_{\rm s}Z_{\rm r}\right]^2}\,{\rm d}\tau\end{aligned} \tag{44}$$

where $Z_{\rm r}=z+h$, $T_{\rm r}=Z/c_0$, and having assumed $v(t)=0$ for $t\le 0$. Moreover,

$$\begin{aligned}\int_0^t\int_{-\infty}^{t'}g^F_{\rm r}(0,z;t'-\tau)\,v(\tau)\,\ell\,{\rm d}\tau\,{\rm d}t'=&-\frac{\hat{G}_{\rm s}V(t-T_{\rm r})}{4\pi\left(2+\hat{G}_{\rm s}\right)Z_{\rm r}}\\&+\frac{c_0\hat{G}_{\rm s}}{2\pi}\int_0^{t-T_{\rm r}}\int_{\tau+T_{\rm r}}^{t}\frac{1}{\left[2c_0(t'-\tau)+\hat{G}_{\rm s}Z_{\rm r}\right]^2}\,{\rm d}t'v(\tau)\,{\rm d}\tau\end{aligned}$$

$$= -\frac{\hat{G}_{\rm s}}{4\pi}\int_0^{t-T_{\rm r}} \frac{v(\tau)}{\left[2c_0(t-\tau)+\hat{G}_{\rm s}Z_{\rm r}\right]}\,{\rm d}\tau \tag{45}$$

where

$$V(t)=\int_0^t v(t')\,{\rm d}t' \tag{46}$$

and having assumed $V(t)=0$ for $t\le 0$. From (43) [by using (44) and (45)], we obtain the z-component of the reflected magnetic field $h_z^{\rm r}$ as

$$h_z^{\rm r}(0,z,t) = -\frac{\hat{G}_{\rm s}}{2\pi\eta_0\left(2+\hat{G}_{\rm s}\right)Z_{\rm r}^2}\,v(t-T_{\rm r})\,\ell + \frac{2\hat{G}_{\rm s}}{\pi\mu_0}\left(1-\frac{\hat{G}_{\rm s}^2}{4}\right)\int_0^{t-T_{\rm r}} \frac{v(\tau)\,\ell}{\left[2(t-\tau)+\hat{G}_{\rm s}T_{\rm r}\right]^3}\,{\rm d}\tau\,. \tag{47}$$

On the other hand, the $g_{\rm inc}^F$ term gives rise to the incident magnetic field and, in particular

$$h_z^{\rm inc}(0,z,t)=\frac{1}{2\pi Z_{\rm t}^2}\left[\frac{v(t-T_{\rm t})\,\ell}{\eta_0}+\frac{V(t-T_{\rm t})\,\ell}{\mu_0 Z_{\rm t}}\right] \tag{48}$$

where $Z_{\rm t}=|z-h|$ and $T_{\rm t}=Z_{\rm t}/c_0$. Therefore,

$$h_z(0,z,t)=h_z^{\rm inc}(0,z,t)+h_z^{\rm r}(0,z,t)\qquad z>0\,. \tag{49}$$

With the same reasoning, considering the transmitted Green function $g_{\rm t}^F$, for $z<0$, we obtain

$$h_z(0,z,t) = \frac{1}{2\pi\mu_0 Z_{\rm t}^3}\,V(t-T_{\rm t})\,\ell + \frac{1}{\pi\eta_0\left(2+\hat{G}_{\rm s}\right)Z_{\rm t}^2}\,v(t-T_{\rm t})\,\ell + \frac{2\hat{G}_{\rm s}}{\pi\mu_0}\left(1-\frac{\hat{G}_{\rm s}^2}{4}\right)\int_0^{t-T_{\rm t}} \frac{v(\tau)\,\ell}{\left[2(t-\tau)+\hat{G}_{\rm s}T_{\rm t}\right]^3}\,{\rm d}\tau\,. \tag{50}$$

IV. Transient Shielding

To assess the transient shielding properties of the screen in the considered configuration the following transient SE (peak-reduction and derivative-reduction efficiencies) are introduced [13]

$${\rm SE}_{\rm PR}^{\rm H}=20\log\frac{\max\limits_t\left|h_z^{\rm inc}(t)\right|}{\max\limits_t|h_z(t)|} \tag{51}$$

$${\rm SE}_{\rm DR}^{\rm H}=20\log\frac{\max\limits_t\left|\frac{\partial h_z^{\rm inc}}{\partial t}\right|}{\max\limits_t\left|\frac{\partial h_z}{\partial t}\right|} \tag{52}$$

where the magnetic fields are assumed to be calculated in $(\rho,z)=(0,-h_2)$.

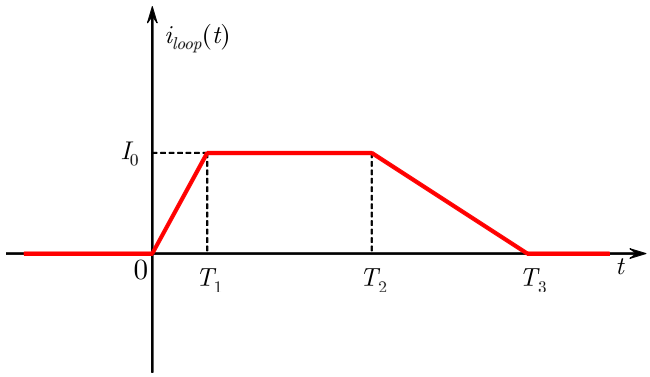

Fig. 2. Transient behavior of the exciting current loop $i_{\rm loop}(t)$.

A simple, but representative, transient current-loop behavior is that reported in Fig. 2 for which

$$i_{\rm loop}(t)\ell=\begin{cases}\frac{I_0}{T_1}\,t & 0<t<T_1\\ I_0 & T_1<t<T_2\\ \frac{(T_3-t)}{(T_3-T_2)}\,I_0 & T_2<t<T_3\\ 0 & \text{elsewhere}\end{cases} \tag{53}$$

and the relevant equivalent voltage is analytically expressed as

$$v(t)\ell=\begin{cases}\frac{V_0\ell}{T_1} & 0<t<T_1\\ 0 & T_1<t<T_2\\ -\frac{V_0\ell}{(T_3-T_2)} & T_2<t<T_3\\ 0 & \text{elsewhere}\end{cases} \tag{54}$$

where $V_0\ell=\mu_0\pi a_1^2 I_0$. With this assumption, from (50), the magnetic field is thus

$$h_z(0,z,t)=h_{z1}(0,z,t)+\frac{2\hat{G}_{\rm s}}{\mu_0\pi}\left(1-\frac{\hat{G}_{\rm s}^2}{4}\right)h_{z2}(0,z,t) \tag{55}$$

where $h_{z1}(0,z,t)=0$ for $t<T_{\rm t}$,

$$h_z(0,z,t)=\frac{V_0\ell}{\pi T_1 Z_{\rm t}^2}\left[\frac{(t-T_{\rm t})}{2\mu_0 Z_{\rm t}}+\frac{1}{\eta_0\left(2+\hat{G}_{\rm s}\right)}\right] \tag{56}$$

for $T_{\rm t}<t<T_1+T_{\rm t}$,

$$h_{z1}(0,z,t)=\frac{V_0\ell}{2\pi\mu_0 Z_{\rm t}^3} \tag{57}$$

for $T_1+T_{\rm t}<t<T_2+T_{\rm t}$,

$$h_{z1}(0,z,t)=\frac{V_0\ell}{2\pi\mu_0 Z_{\rm t}^3}\left[\frac{T_3+T_{\rm t}-t}{(T_3-T_2)}\right] - \frac{1}{\pi\eta_0\left(2+\hat{G}_{\rm s}\right)Z_{\rm t}^2}\,\frac{V_0\ell}{(T_3-T_2)} \tag{58}$$

for $T_2+T_{\rm t}<t<T_3+T_{\rm t}$, and $h_{z1}(0,z,t)=0$ for $t>T_3+T_{\rm t}$.

Moreover, it results $h_{z2}=0$ for $t<T_\mathrm{t}$,

$$h_{z2}(0,z,t)=\frac{V_0\ell}{4T_1}\left[\frac{1}{\left(2+\hat{G}_\mathrm{s}\right)^2T_\mathrm{t}^2}-\frac{1}{\left(2t+\hat{G}_\mathrm{s}T_\mathrm{t}\right)^2}\right] \tag{59}$$

for $T_\mathrm{t}<t<T_1+T_\mathrm{t}$,

$$h_{z2}(0,z,t)=\frac{V_0\ell}{4T_1}\cdot\left\{\frac{1}{\left[2\left(t-T_1\right)+\hat{G}_\mathrm{s}T_\mathrm{t}\right]^2}-\frac{1}{\left(2t+\hat{G}_\mathrm{s}T_\mathrm{t}\right)^2}\right\} \tag{60}$$

for $T_1+T_\mathrm{t}<t<T_2+T_\mathrm{t}$,

$$h_{z2}(0,z,t)=\frac{V_0\ell}{4T_1}\cdot\left\{\frac{1}{\left[2\left(t-T_1\right)+\hat{G}_\mathrm{s}T_\mathrm{t}\right]^2}-\frac{1}{\left(2t+\hat{G}_\mathrm{s}T_\mathrm{t}\right)^2}\right\}-\frac{V_0\ell}{4\left(T_3-T_2\right)}\left\{\frac{1}{\left(2+\hat{G}_\mathrm{s}\right)^2T_\mathrm{t}^2}-\frac{1}{\left[2\left(t-T_2\right)+\hat{G}_\mathrm{s}T_\mathrm{t}\right]^2}\right\} \tag{61}$$

for $T_2+T_\mathrm{t}<t<T_3+T_\mathrm{t}$, and

$$h_{z2}(0,z,t)=\frac{V_0\ell}{4T_1}\cdot\left\{\frac{1}{\left[2\left(t-T_1+T_\mathrm{t}\right)+\hat{G}_\mathrm{s}T_\mathrm{t}\right]^2}-\frac{1}{\left(2t+\hat{G}_\mathrm{s}T_\mathrm{t}\right)^2}\right\}-\frac{V_0\ell}{4\left(T_3-T_2\right)}\cdot\left\{\frac{1}{\left[2\left(t-T_3\right)+\hat{G}_\mathrm{s}T_\mathrm{t}\right]^2}-\frac{1}{\left[2\left(t-T_2\right)+\hat{G}_\mathrm{s}T_\mathrm{t}\right]^2}\right\} \tag{62}$$

for $t>T_3+T_\mathrm{t}$.

On the other hand, the incident field can be evaluated as $h_z^{\mathrm{inc}}=h_{z1}$ by simply letting $\hat{G}_\mathrm{s}=0$ in (56)–(58).

V. Numerical Results

We consider two exciting circular electric current loops with a transient waveform as in Fig. 2 and with the following parameters: $T_1=6u$, $T_2=16u$, and $T_3=20u$, where u equals 10^{-4} s (current #1 - slow transient) and 10^{-6} s (current #2 - fast transient), respectively. The frequency spectra of the currents are reported in Fig. 3. We also consider two shields having conductivities $\sigma=37$ MS/m (aluminum) and $\sigma=6.3$ MS/m (stainless steel), respectively, with different thicknesses d; in both cases, the electric permittivity and magnetic permeability of the shields have been assumed to be those of vacuum, i.e., $\varepsilon=\varepsilon_0$ and $\mu=\mu_0$. The circular current loop has a radius $a=30$ cm and is placed at a distance $h=30$ cm from the shields.

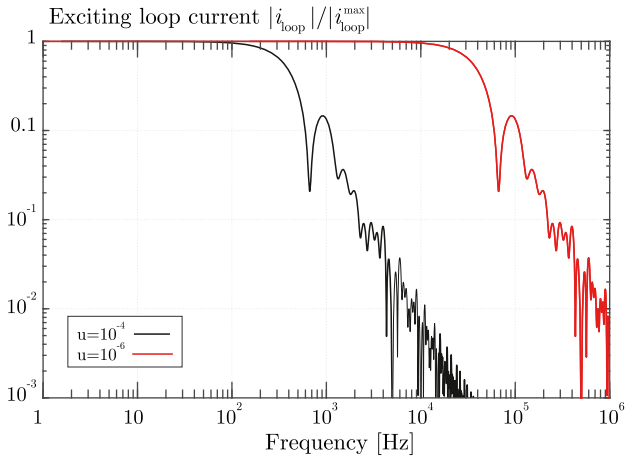

Fig. 3. Frequency spectrum of two exciting loop currents with slow transient waveform (*black line*) and fast transient waveform (*red line*).

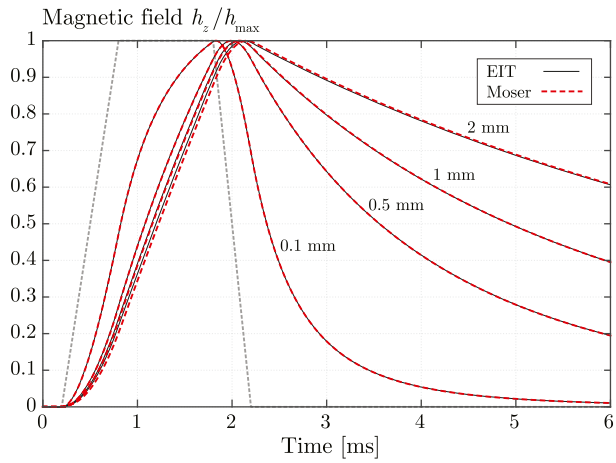

Fig. 4. Normalized magnitude of the z-component of the magnetic field produced at $z=-30$ cm by a circular current loop with radius $a=30$ cm placed at a distance $h=30$ cm from a screen with $\sigma=37$ MS/m (aluminum), for different values of the screen thickness d: case of a slow transient loop current #1. *Legend:* solid black lines—EIT; red dashed lines—Moser formulation; gray dashed line—waveform of the current loop $i_{\mathrm{loop}}(t)$.

Figs. 4 and 5 show the normalized magnitudes of the z-component of the magnetic field computed at $z=-30$ cm as a function of time, in the case of the slow transient current loop #1 for the two considered shields, for different screen thicknesses d. The results have been computed through the proposed EIT (*solid black lines*) and the theory proposed by Moser [7] (*dashed red lines*). The results confirm the great accuracy of the proposed approach as far as the shield can be considered electrically thin according to (3). Furthermore, they show that, for observation points placed on the rotational axis of the system, representing the loop source through a magnetic dipole is a valid approximation also when the source radius a is not small with respect to the source distance from the screen h (in the shown results $a=h$).

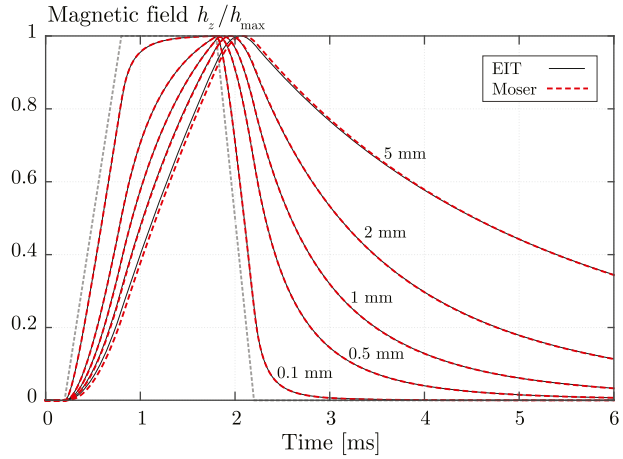

Fig. 5. Same as in Fig. 4, for a screen with $\sigma = 6.3$ MS/m (stainless steel).

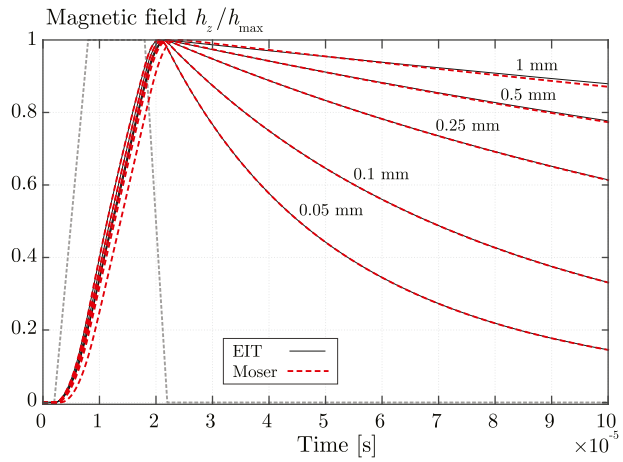

Fig. 6. Same as in Fig. 5 for a fast transient current loop #2.

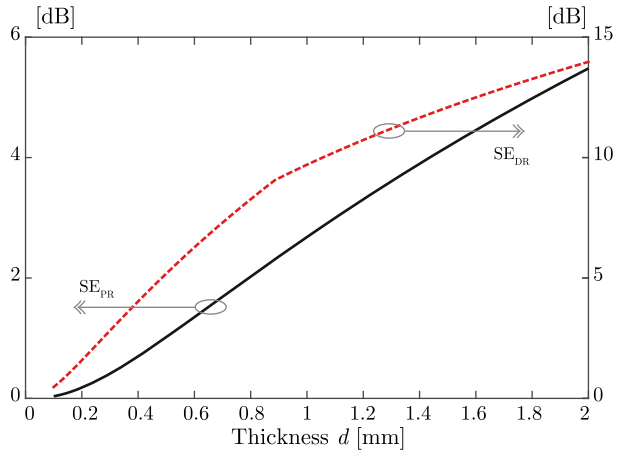

Fig. 7. Peak-reduction SE^H_{PR} and derivative-reduction SE^H_{DR} as functions of the thickness d for the stainless-steel shield in the case of the current loop #1.

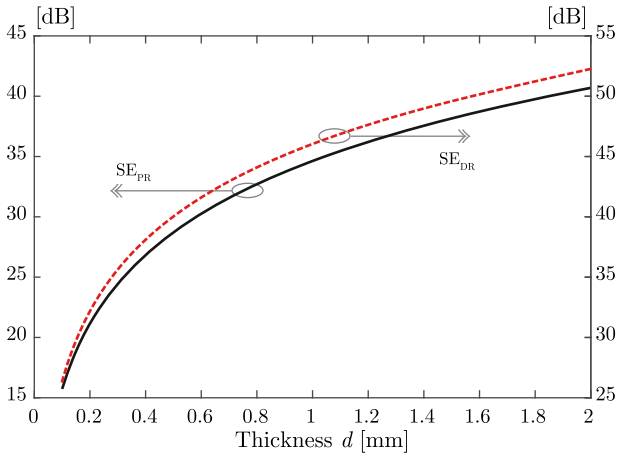

Fig. 8. Peak-reduction SE^H_{PR} and derivative-reduction SE^H_{DR} as functions of the thickness d for the stainless-steel shield in the case of the current loop #2.

It is worth noting that both the spectral integrals occurring in Moser's frequency-domain formulation and the inverse Fourier-transform integrals required to obtain the relevant TD results are defined over semi-infinite domains and are in general both oscillating and slowly converging at infinity. Their numerical evaluation is, thus, both nontrivial and computationally intensive if compared with the proposed formulation, which involves only single nonoscillating integrals over finite intervals. The latter are even amenable to closed-form evaluation for simple source waveforms, as shown in Section IV; even when this is not possible, the reduction in computational time afforded by the proposed formulation is on the order of 10^2 or more.

By increasing the screen thickness d, the distortion of the field shape increases due to the effect of the dispersion and losses that the field undergoes while passing through the shield. For clarity, the normalized waveform of the exciting current $i_{loop}(t)$ is also reported (*dashed gray lines*) to visually assess the field components' distortion.

Fig. 6 shows the normalized magnitudes of the z-magnetic field in the same previous setup for the stainless-steel shield in the case of the fast transient current loop #2.

For the same shield, in Figs. 7 and 8, we report the peak-reduction SE SE^H_{PR} and the derivative-reduction SE SE^H_{DR} under the transient current loops #1 and #2, respectively, for different thicknesses d. Both the SE obviously increase by increasing the thickness d; it is worthy pointing out that, as stated in previous publications [14], [41], [42], [43], SE^H_{DR} is usually larger than SE^H_{PR}, and the present results confirm this trend.

VI. Conclusion

A TD version of the EIT has been presented to solve a canonical shielding problem directly in the TD. The problem basically consists in evaluating the TD magnetic field produced by a small circular current loop with a transient waveform in the presence of a parallel planar thin conductive sheet. It has been shown that the TD EIT analytically solves the problem in a considerably simple way and the transient field components can be easily computed through the TD Green function derived in closed form. In fact, the final integrals expressing such components may be computed

analytically giving a closed-form solution (an example is provided considering the z-component of the magnetic field). We have shown that for simple transient waveforms of the exciting currents, the dominant component of the on-axis magnetic field can also be expressed in a closed form and the derived results allow for evaluating the transient SE of different configurations. Comparisons with numerical brute-force techniques based on inverse Fourier transforms confirm the validity and the efficiency of the proposed formulation.

The proposed approach can also be used to study the transient excitation of a thin conductive screen by a vertical electric dipole, which would excite a TM rather than a TE field, as well as the more complex case of a shielding configuration involving two coplanar loops orthogonal to the screen. In the latter case, the problem would not be rotationally symmetric anymore and the field would have a hybrid polarization, which requires to consider both the TE and the TM reflection and transmission coefficients of the screen. Work is in progress on the analysis of these configurations as well as on their application to the transient analysis of grounding systems.

Appendix
Derivation of (21)

The integral in (20) can first be rewritten as

$$G_{\mathrm{c}}(q,t) = \frac{c_0}{2\pi} \cdot \int_{-\infty}^{+\infty} \frac{\mathrm{e}^{-\mathrm{j}\sqrt{k_0^2 r_+^2 - 2\mathrm{j}(z+h)\frac{2qk_0}{\hat{G}_{\mathrm{s}}} - \frac{4q^2}{\hat{G}_{\mathrm{s}}^2}}}}{4\pi\sqrt{k_0^2 r_+^2 - 2\mathrm{j}\,(z+h)\,\frac{2qc_0k_0}{\hat{G}_{\mathrm{s}}} - \frac{4q^2}{\hat{G}_{\mathrm{s}}^2}}}\ \mathrm{e}^{\mathrm{j}c_0k_0t}\ k_0\,\mathrm{d}k_0. \tag{63}$$

With the change of variable $k_0 = k + \mathrm{j}\alpha_+ q$ and some algebra, the integral in (63) becomes

$$G_{\mathrm{c}}(q,t) = \frac{c_0}{8\pi^2}\ \mathrm{e}^{-c_0\alpha_+ qt} \cdot \int_{-\infty-\mathrm{j}\alpha_+ q}^{+\infty-\mathrm{j}\alpha_+ q} \frac{\mathrm{e}^{\mathrm{j}kc_0t - \mathrm{j}\sqrt{k^2r_+^2 - \frac{4q^2\rho^2}{\hat{G}_{\mathrm{s}}^2 r_+^2}}}}{\sqrt{k^2r_+^2 - \frac{4q^2\rho^2}{\hat{G}_{\mathrm{s}}^2 r_+^2}}}\ (k + \mathrm{j}\alpha_+ q)\ \mathrm{d}k. \tag{64}$$

The determination of the square root in (64) is chosen so that $\mathrm{Im}\{\sqrt{\cdot}\} \leq 0$. It should be noted that the square-root function introduces branch points on the real k-axis at $k_{1,2}^{\mathrm{bp}} = \pm 2q\rho/(\hat{G}_{\mathrm{s}} r_+^2)$: the relevant branch cut can be chosen as the segment joining the two branch points and passing through the origin.

The integral in (64) vanishes for $c_0 t < r_+$, according to Cauchy's integral formula (the integration path can be closed at infinity in the lower half-plane without capturing any pole). When $c_0 t > r_+$, the integration path can be shifted below the real k-axis, and with the change of variable $k = -\mathrm{j}s$, we have

$$G_{\mathrm{c}}(q,t) = \frac{c_0}{4\pi r_+}\ \mathrm{e}^{-\alpha_+ qc_0t}\ \frac{1}{2\pi\mathrm{j}} \int_{-\mathrm{j}\infty}^{+\mathrm{j}\infty} \frac{\mathrm{e}^{-\sqrt{s^2 + \left(\frac{2q\rho}{\hat{G}_{\mathrm{s}} r_+^2}\right)^2}\, r_+}}{\sqrt{s^2 + \left(\frac{2q\rho}{\hat{G}_{\mathrm{s}} r_+^2}\right)^2}} \cdot (s - \alpha_+ q)\ \mathrm{e}^{sc_0t}\ \mathrm{d}s. \tag{65}$$

It is then easy to recognize that

$$G_{\mathrm{c}}(q,t) = \frac{c_0}{4\pi r_+}\ \mathrm{e}^{-\alpha_+ qc_0t} \left[\frac{\partial}{\partial\,(c_0t)}\, g_1(q,t) - \alpha_+ q g_1(q,t)\right] \tag{66}$$

where

$$g_1(q,t) = \frac{1}{2\pi\mathrm{j}} \int_{-\mathrm{j}\infty}^{+\mathrm{j}\infty} \frac{\mathrm{e}^{-\sqrt{s^2 + \left(\frac{2q\rho}{\hat{G}_{\mathrm{s}} r_+^2}\right)^2}\, r_+}}{\sqrt{s^2 + \left(\frac{2q\rho}{\hat{G}_{\mathrm{s}} r_+^2}\right)^2}}\ \mathrm{e}^{sc_0t}\ \mathrm{d}s = L^{-1}\left\{\frac{\mathrm{e}^{-r_+\sqrt{s^2 + \left(\frac{2q\rho}{\hat{G}_{\mathrm{s}} r_+^2}\right)^2}}}{\sqrt{s^2 + \left(\frac{2q\rho}{\hat{G}_{\mathrm{s}} r_+^2}\right)^2}}\right\}\Bigg|_{\tau = c_0t}. \tag{67}$$

Now, from the integral identity [40, 6.616.2], we also have

$$\frac{\mathrm{e}^{-\eta\sqrt{a^2+b^2}}}{\sqrt{a^2+b^2}} = \int_0^{+\infty} \mathrm{J}_0\left(b\sqrt{y^2-\eta^2}\right) H(y-\eta)\ \mathrm{e}^{-ay}\ \mathrm{d}y. \tag{68}$$

From (68), we can, thus, recognize

$$L^{-1}\left\{\frac{\mathrm{e}^{-\eta\sqrt{a^2+b^2}}}{\sqrt{a^2+b^2}}\right\} = \mathrm{J}_0\left(b\sqrt{y^2-\eta^2}\right) H(y-\eta) \tag{69}$$

so that from (67) and (69), we obtain

$$g_1(q,t) = \mathrm{J}_0\left(\frac{2q\rho}{\hat{G}_{\mathrm{s}} r_+^2}\sqrt{(c_0t)^2 - r_+^2}\right) H(c_0t - r_+). \tag{70}$$

From (66), we, thus, have

$$G_{\mathrm{c}}(q,t) = \frac{c_0}{4\pi r_+}\ \mathrm{e}^{-\alpha_+ qc_0t} \cdot \left\{\delta(c_0t - r_+)\,\mathrm{J}_0\left(\frac{2q\rho}{\hat{G}_{\mathrm{s}} r_+^2}\sqrt{(c_0t)^2 - r_+^2}\right) - \left[\mathrm{J}_1\left(\frac{2q\rho}{\hat{G}_{\mathrm{s}} r_+^2}\sqrt{(c_0t)^2 - r_+^2}\right)\frac{2q\rho}{\hat{G}_{\mathrm{s}} r_+^2}\,\frac{c_0^2 t}{\sqrt{(c_0t)^2 - r_+^2}} + \alpha_+ q\,\mathrm{J}_0\left(\frac{2q\rho}{\hat{G}_{\mathrm{s}} r_+^2}\sqrt{(c_0t)^2 - r_+^2}\right)\right] H(c_0t - r_+)\right\}. \tag{71}$$

By letting $\beta_+ = 2\rho\sqrt{(c_0t)^2 - r_+^2}\,/(\hat{G}_{\mathrm{s}} r_+^2)$ from (71), we finally obtain (21).

REFERENCES

[1] NSA, "SpecificationNSA 94-106: Specification for shielded enclosures," Nat. Secur. Agency, Fort Meade, MD, USA, 1994.

[2] J. Catrysse, F. Vanhee, D. Pissoort, and S. Celozzi, "Differences between NSA 94-106 and IEEE 299 LF magnetic shielding measurements," in *Proc. IEEE Int. Symp. Electromagn. Compat.*, 2015, pp. 13–16.

[3] S. Levy, "Electromagnetic shielding effect of an infinite plane conducting sheet placed between circular coaxial coils," *Proc. Inst. Radio Engineers*, vol. 24, no. 6, pp. 923–941, Jun. 1936.

[4] J. R. Moser, "Low-frequency shielding of a circular loop electromagnetic field source," *IEEE Trans. Electromagn. Compat.*, vol. 9, no. 1, pp. 6–18, Mar. 1967.

[5] P. R. Bannister, "New theoretical expressions for predicting shielding effectiveness for the plane shield case," *IEEE Trans. Electromagn. Compat.*, vol. EMC-10, no. 1, pp. 2–7, Mar. 1968.

[6] P. R. Bannister, "Further notes for predicting shielding effectiveness for the plane shield case," *IEEE Trans. Electromagn. Compat.*, vol. EMC-11, no. 2, pp. 50–53, May 1969.

[7] J. R. Moser, "Low-frequency low-impedance electromagnetic shielding," *IEEE Trans. Electromagn. Compat.*, vol. 30, no. 3, pp. 202–210, Aug. 1988.

[8] R. Hansen and J. R. Moser, "Loop-shield-loop shielding effectiveness," *IEEE Trans. Electromagn. Compat.*, vol. 41, no. 2, pp. 144–146, May 1999.

[9] G. Lovat, P. Burghignoli, R. Araneo, and S. Celozzi, "Magnetic shielding of planar metallic screens: A new analytical closed-form solution," *IEEE Trans. Electromagn. Compat.*, vol. 62, no. 5, pp. 1884–1888, Oct. 2020.

[10] G. Lovat, P. Burghignoli, R. Araneo, E. Stracqualursi, and S. Celozzi, "Analytical evaluation of the low-frequency magnetic shielding of thin planar magnetic and conductive screens," *IEEE Trans. Electromagn. Compat.*, vol. 63, no. 1, pp. 308–312, Feb. 2021.

[11] G. Lovat, P. Burghignoli, R. Araneo, and S. Celozzi, "Exact closed-form shielding effectiveness of planar screens with small parallel loops," *IEEE Trans. Electromagn. Compat.*, vol. 64, no. 5, pp. 1694–1702, Aug. 2022.

[12] C. Jiao et al., "Low-frequency magnetic shielding of planar shields: A unified wave impedance formula for the transmission line analogy," *IEEE Trans. Electromagn. Compat.*, vol. 63, no. 4, pp. 1046–1057, Aug. 2021.

[13] S. Celozzi and R. Araneo, "Alternative definitions for the time-domain shielding effectiveness of enclosures," *IEEE Trans. Electromagn. Compat.*, vol. 56, no. 2, pp. 482–485, Apr. 2014.

[14] G. Lovat, R. Araneo, and S. Celozzi, "Near-field time-domain shielding effectiveness of thin conductive screens," *Progr. Electromagn. Res.*, vol. 146, pp. 47–56, 2014.

[15] P. Burghignoli, G. Lovat, R. Araneo, and S. Celozzi, "Time-domain shielding of a thin conductive sheet in the presence of vertical dipoles," *IEEE Trans. Electromagn. Compat.*, vol. 60, no. 1, pp. 157–165, Feb. 2018.

[16] G. Lovat, R. Araneo, P. Burghignoli, and S. Celozzi, "The electromagnetic effects of pulsed horizontal dipoles on a thin conductive sheet: Time-domain analysis," *IEEE Trans. Electromagn. Compat.*, vol. 62, no. 2, pp. 443–450, Apr. 2019.

[17] G. Lovat and R. Araneo, "Semi-analytical representation of the two-dimensional time-domain Green's function of a graphene sheet in the intraband regime," *IEEE Trans. Nanotech.*, vol. 14, no. 4, pp. 681–688, Jul. 2015.

[18] G. Lovat, P. Burghignoli, R. Araneo, and S. Celozzi, "Time-domain Green's function for a vertical dipole above a graphene sheet," *IEEE Trans. Nanotech.*, vol. 17, no. 4, pp. 841–851, Jul. 2018.

[19] P. Burghignoli, G. Lovat, R. Araneo, and S. Celozzi, "Pulsed vertical dipole response of a thin sheet with high-contrast dielectric and conductive properties," *IEEE Trans. Antennas Propag.*, vol. 66, no. 1, pp. 217–225, Jan. 2018.

[20] L. Cagniard, *Réflexion et réfraction des ondes séismiques progressives*. Paris, France: Gauthier-Villars, 1939.

[21] A. T. De Hoop and H. Frankena, "Radiation of pulses generated by a vertical electric dipole above a plane, non-conducting, Earth," *Appl. Sci. Res. B*, vol. 8, no. 1, Jan. 1960, Art. no. 369.

[22] M. Štumpf, A. T. D. Hoop, and G. A. E. Vandenbosch, "Generalized ray theory for time-domain electromagnetic fields in horizontally layered media," *IEEE Trans. Antennas Propag.*, vol. 61, no. 5, pp. 2676–2687, May 2013.

[23] L. Tsang and J. A. Kong, "Modified modal theory of transient response in layered media," *J. Math. Phys.*, vol. 20, no. 6, pp. 1170–1182, 1979.

[24] P. Burghignoli, G. Lovat, R. Araneo, and S. Celozzi, "Time-domain surface plasmon polaritons on a graphene sheet," *Phys. Rev. B*, vol. 97, no. 24, 2018, Art. no. 245418.

[25] R. Haddon, "Exact evaluation of the response of a layered elastic medium to an explosive point source using leaking modes," *Bull. Seismological Soc. Amer.*, vol. 76, no. 6, pp. 1755–1775, Jun. 1986.

[26] G. W. Hanson, A. B. Yakovlev, and J. Hao, "Leaky-wave analysis of transient fields due to sources in planarly layered media," *IEEE Trans. Antennas Propag.*, vol. 51, no. 2, pp. 146–159, Feb. 2003.

[27] L. B. Felsen and F. Niu, "Spectral analysis and synthesis options for short pulse radiation from a point dipole in a grounded dielectric layer," *IEEE Trans Antennas Propag.*, vol. 41, no. 6, pp. 747–754, Jun. 1993.

[28] F. Niu and L. B. Felsen, "Time-domain leaky modes on layered media: Dispersion characteristics and synthesis of pulsed radiation," *IEEE Trans. Antennas Propag.*, vol. 41, no. 6, pp. 755–761, Jun. 1993.

[29] F. Niu and L. B. Felsen, "Asymptotic analysis and numerical evaluation of short pulse radiation from a point dipole in a grounded dielectric layer," *IEEE Trans. Antennas Propag.*, vol. 41, no. 6, pp. 762–769, Jun. 1993.

[30] I. Lindell and E. Alanen, "Exact image theory for the Sommerfeld half-space problem, Part I: Vertical magnetic dipole," *IEEE Trans. Antennas Propag.*, vol. 32, no. 2, pp. 126–133, Feb. 1984.

[31] I. Lindell and E. Alanen, "Exact image theory for the Sommerfeld half-space problem, part II: Vertical electrical dipole," *IEEE Trans. Antennas Propag.*, vol. 32, no. 8, pp. 841–847, Aug. 1984.

[32] I. Lindell and E. Alanen, "Exact image theory for the Sommerfeld half-space problem, Part III: General formulation," *IEEE Trans. Antennas Propag.*, vol. 32, no. 10, pp. 1027–1032, Oct. 1984.

[33] E. F. Kuester and D. C. Chang, "Evaluation of sommerfeld integrals associated with dipole sources above earth," Electromagn. Lab., Dept. Elect. Eng., Univ. Colorado, Boulder, CO, USA, Sci. Rep. 43, 1979.

[34] K. Michalski and J. Mosig, "The sommerfeld half-space problem revisited: From radio frequencies and Zenneck waves to visible light and Fano modes," *J. Electromagn. Waves Appl.*, vol. 30, no. 1, pp. 1–42, 2016.

[35] K. I. Nikoskinen and I. V. Lindell, "Time-domain analysis of the sommerfeld VMD problem based on the exact image theory," *IEEE Trans. Antennas Propag.*, vol. 38, no. 2, pp. 241–250, Feb. 1990.

[36] R. Araneo and S. Celozzi, "Exact solution of the low-frequency coplanar loops shielding configuration," *IEE Proc.-Sci., Meas. Technol.*, vol. 149, no. 1, pp. 37–44, 2002.

[37] G. Lovat, P. Burghignoli, R. Araneo, E. Stracqualursi, and S. Celozzi, "Closed-form LF magnetic shielding effectiveness of thin planar screens in coplanar loops configuration," *IEEE Trans. Electromagn. Compat.*, vol. 63, no. 2, pp. 631–635, Apr. 2021.

[38] R. Araneo and S. Celozzi, "Transient behavior of wind towers grounding systems under lightning strikes," *Int. J. Energy Environ. Eng.*, vol. 7, pp. 235–247, 2016.

[39] W. C. Chew, *Waves and Fields in Inhomogenous Media*. Piscataway, NJ, USA: Wiley, 1999.

[40] I. S. Gradshteyn and I. M. Ryzhik, *Table of Integrals, Series, and Products*, 7th ed. Amsterdam, The Netherlands: Elsevier/Acad. Press, 2007.

[41] S. Celozzi and R. Araneo, "TD-shielding effectiveness of enclosures in presence of ESD," in *Proc. Int. Symp. Electromagn. Compat.*, 2013, pp. 541–544.

[42] R. Araneo and S. Celozzi, "Toward a definition of the shielding effectiveness in the time - domain," in *Proc. IEEE Int. Symp. Electromagn. Compat.*, 2013, pp. 113–117.

[43] R. Araneo, G. Attolini, G. Lovat, and S. Celozzi, "A global approach to time-domain shielding problems," in *Proc. IEEE Int. Symp. Electromagn. Compat.*, 2014, pp. 86–90.

Open Access provided by 'Università degli Studi di Roma "La Sapienza" 2' within the CRUI CARE Agreement